The Influence of α- and γ-Al_2O_3 Phases on the Thermoelectric Properties of Al-doped ZnO

Han, Li; Van Nong, Ngo; Le, Thanh Hung; Holgate, Tim; Pryds, Nini; Ohtaki, Michitaka ; Linderoth, Søren

Published in:
Journal of Alloys and Compounds

Link to article, DOI:
10.1016/j.jallcom.2012.12.091

Publication date:
2013

The Influence of α- and γ-Al_2O_3 Phases on the Thermoelectric Properties of Al-doped ZnO

Li Han, Ngo Van Nong, Le Thanh Hung, Tim Holgate, Nini Pryds, Michitaka Ohtaki, Søren Linderoth

PII: S0925-8388(12)02315-8
DOI: http://dx.doi.org/10.1016/j.jallcom.2012.12.091
Reference: JALCOM 27531

To appear in:

Received Date: 7 November 2012
Revised Date: 17 December 2012
Accepted Date: 18 December 2012

Please cite this article as: L. Han, N.V. Nong, L.T. Hung, T. Holgate, N. Pryds, M. Ohtaki, S. Linderoth, The Influence of α- and γ-Al_2O_3 Phases on the Thermoelectric Properties of Al-doped ZnO, (2012), doi: http://dx.doi.org/10.1016/j.jallcom.2012.12.091

The Influence of α- and γ-Al_2O_3 Phases on the Thermoelectric Properties of Al-doped ZnO

Li Han, [a *] Ngo Van Nong, [a] Le Thanh Hung, [a] Tim Holgate,[a] Nini Pryds, [a] Michitaka Ohtaki[b] and Søren Linderoth[a]

[a] *Department of Energy Conversion and Storage, Technical University of Denmark, DTU Risø Campus, Frederiksborgvej 399, 4000 Roskilde, Denmark.*

[b] *Department of Molecular and Materials Sciences, Interdisciplinary Graduate School of Engineering Sciences, Kyushu University, 6-1 Kasugakoen, Kasuga, Fukuoka 816-8580, Japan*

Abstract:

A systematic investigation on the microstructure and thermoelectric properties of Al-doped ZnO using α- and γ-Al_2O_3 as dopants was conducted in order to understand the doping effect and its mechanism. The samples were prepared by the spark plasma sintering technique from precursors calcined at various temperatures. Clear differences in microstructure and thermoelectric properties were observed between the samples doped with α- and γ-Al_2O_3. At any given calcination temperature, γ-Al_2O_3 resulted in the formation of a larger amount of the $ZnAl_2O_4$ phase in the Al-doped ZnO samples. The average grain size was found to be smaller for the γ-Al_2O_3-doped samples than that for the α-Al_2O_3-doped ones under the same sintering condition. It is proposed that the $ZnAl_2O_4$ phase is the reason for the observed suppression of grain growth and also for the slightly reduced lattice thermal conductivity exhibited by these samples. The γ-Al_2O_3 promoted the substitution for donor impurities in ZnO, thus resulting in shrinkage of the unit cell volume and an increase in the electrical conductivity compared with the α-Al_2O_3-doped ZnO. At a calcination temperature of 1173K, the γ-Al_2O_3-doped sample showed a ZT value of 0.17 at 1173K, which is 27% higher than that of the α-Al_2O_3-doped sample.

Key words: thermoelectric oxide, Al-doped ZnO, α- and γ-Al_2O_3, $ZnAl_2O_4$ formation kinetics.

1. Introduction

Thermoelectric oxide materials are strong candidates for high temperature power generation from waste heat. The promising high temperature n-type

* Corresponding author at: DTU Energy Conversion, DTU Risø Campus, Frederiksborgvej 399, 4000 Roskilde, Denmark

E-mail address: ihan@dtu.dk

thermoelectric properties of Al-doped ZnO were first brought to the public sight by Ohtaki et al. in 1996 [1]. Recently, a figure-of-merit, ZT of 0.44 at 1000 K was obtained for nanostructured Al-doped ZnO [2], and again this showed the possibility of using ZnO for low-cost practical waste heat harvesting. In the last few years, intensive investigations have been targeted to improve the thermoelectric properties and the preparation conditions of Al-doped ZnO [3,4,5,18], but little attention has been paid to the choice of which phases of Al_2O_3 should be used as the dopant. This is probably one of the reasons for the controversial results reported by many research groups on the thermoelectric performance of Al-doped ZnO. Therefore, it is noteworthy to investigate systematically the influences of using different phases of Al_2O_3 as dopants on the thermoelectric properties of Al-doped ZnO. In fact, the α- and γ-phases of Al_2O_3 have different crystal structures and physical properties with their specific reaction kinetics with ZnO [6,7,8]. Moreover, the phase transition of Al_2O_3 is temperature dependent, suggesting that the synthesis temperature of Al-doped ZnO is crucial and can result in different material properties.

From this point of view, we have conducted a systematic investigation of the microstructure and the thermoelectric properties of Al-doped ZnO synthesized by various heat treatments using two different phases of Al_2O_3 as dopants: γ-Al_2O_3 with a defect spinel structure and α-Al_2O_3 with the corundum structure. We observed a noticeable difference in the microstructure and thermoelectric properties between α- and γ-Al_2O_3-doped ZnO when the synthesis temperature was lower than 1273 K. The correlations between the thermoelectric properties, microstructure evolutions, and the solid state reaction kinetics of the secondary phases are discussed herein.

2. Experimental Procedure

The starting materials used in these investigations are: ZnO (99+% 40-100 nm APS powder, Alfa-Aesar), γ-Al_2O_3 (99.5% 45-55 nm APS Powder, Alfa-Aesar), and α-Al_2O_3 (99.5% 0.9-2.2 Micron APS Powder, Alfa-Aesar).

The synthesis of Al-doped ZnO ceramics: Aluminum oxide (γ-Al_2O_3 or α-Al_2O_3) was mixed with ZnO at a molar ratio of 1:98 (the atomic ratio of Al:Zn = 2:98) by ethanol-aided roll milling using ceramic balls for 24 h. The resulting mixtures were then dried at room temperature for 24 h followed by further drying

at 403 K for 3 h. The dried powders were put into porcelain boats and calcined at various temperatures (973, 1073, 1173, and 1273 K) under N_2 for 1 h. After calcination, the powders were sieved using a 300 mesh sieve, corresponding to a mean particle size of 48μm. The precursors were densified using optimized conditions into compact bulk pellets by spark plasma sintering (SPS) at 1173 K for 5 min in argon under a uniaxial pressure of 50 MPa. The six sintered samples are denoted as γ-973, α-1073, γ-1073, α-1173, γ-1173, α-1273 according to the phase of Al_2O_3 used and the calcination temperatures. These samples and their precursors were examined by power X-ray diffraction (XRD) on a Bruker D8 diffractometer (Bruker, Germany) using Cu-Kα radiation. The density of the samples was measured on an AccuPyc-1340 Pycnometer. A scanning electron microscope (SEM) (Supra, Carl Zeiss, Inc. Germany) equipped with an EDX spectrometer was used to observe the microstructures of the samples. The measurements of the electrical resistivity and the Seebeck coefficient were carried out on an ULVAC-RIKO ZEM-3 from room temperature up to 1173 K under a low pressure of helium atmosphere. The thermal conductivity was determined from the thermal diffusivity obtained by the laser flash method (a Netzch FLA-457) and the specific heat capacity calculated by the Dulong-Petit relation.

3. Results and discussion

The relative density of the bulk sintered ZnO samples doped with α/γ-Al_2O_3 was found to be all above 95% regardless of the calcination temperature. X-ray diffraction analysis for these samples showed that most of the observed XRD peaks (see Fig. 1a) are assigned to those of pure ZnO phase (ICDD card PDF#36-1451). It also reveals in the inset of Fig. 1 that the peak at $2\theta = 36.83°$ assigned to the strongest peak of $ZnAl_2O_4$ gahnite phase [14]. Comparing this peak over the samples, it seems as if those peaks of the α-1073 and γ-973 samples are more diffused than those of the samples with higher calcination temperature. The cell volume monotonically decreased with increasing calcination temperature for both α- and γ-Al_2O_3-doped samples (see Fig. 1b). The ionic radius of Al^{3+} (0.039 nm, 4-fold coordination) is smaller than that of Zn^{2+} (0.060 nm, 4-fold coordination) [17], suggesting that the decrease of the unit cell volume may originate from the substitutions of Al^{3+} at Zn-sites promoted by the elevated calcination temperature.

It should also be noted that the unit cell volume was smaller for the γ-1073 and γ-1173 samples than that for the α-1073 and α-1173 samples, respectively.

Fig. 2a-f shows the SEM micrographs of fracture surfaces and the EDX analysis from a selected area of α/γ-Al_2O_3-doped ZnO samples sintered by SPS. Fig. 2a-e reveal that besides the ZnO grains with the size of several micrometers, there exist some interspersed nano-sized grains, which precipitate within the ZnO grain interiors or at the grain boundaries. An EDX line scan was taken across the nanoprecipitates (see Figure 2e, f), showing that these nano-grains have enriched Al concentrations. This observation, together with the $ZnAl_2O_4$ gahnite phase detected by XRD, suggests the formation of $ZnAl_2O_4$ precipitates in these samples. A difference in the grain growth was also clearly observed as the calcination temperature increased. At the same calcination temperature the γ-Al_2O_3-doped samples have smaller average grain sizes (~1μm) than those of the α-Al_2O_3-doped samples (~1.5μm), as shown in Figs. 2b and 2c. This difference in grain size would be caused by the boundary pinning effect of the $ZnAl_2O_4$ nanoprecipitates during grain growth [9]. These results indicate that the formation rate of $ZnAl_2O_4$ is closely correlated to the phases of the Al_2O_3 precursors, and this will be discussed in the following section with relation to the kinetic calculation.

Fig. 3 shows the temperature dependence of the electrical conductivity (σ) of α/γ-Al_2O_3-doped ZnO samples. All the investigated samples showed a semiconducting behavior over the whole measured temperature range, i.e. the electrical conductivity increases with increasing temperature. The calculated activation energy for electronic conduction of the α-1073 sample changed from ~17 meV to ~304 meV at and above 770 K. With increasing calcination temperature, this change became less pronounced suggesting that more carriers are available for conduction. For both the α- and the γ-Al_2O_3-doped ZnO samples, the electrical conductivity increased with increasing calcination temperature. The σ values of the γ-1073 and γ-1173 samples are notably higher than those of the α-1073 and α-1173 samples, respectively. Shown in the inset of Fig. 3 is the electrical conductivity, which was extracted from the data at 1173 K, as a function of the calcination temperature. It appears that the change of σ is consistent with the change of the unit cell volume (Fig. 1b), which could be attributed to the Al substitution at the Zn-site according to the following equation [10]:

$$Al_2O_3 \xrightarrow{Zn\,O} 2Al_{Zn}^{\cdot} + 2e^{'} + 2O_o^X + \frac{1}{2}O_2 \uparrow \qquad (1)$$

From Eq. 1, one can see that the substitution of Zn^{2+} by Al^{3+} is the reason for the unit cell volume shrinkage which may result in the increase in the donor impurity concentration [11], thus providing excess charged carriers available for electrical conduction.

Fig. 4 shows the temperature dependence of the Seebeck coefficients, *S*, of the α/γ-Al_2O_3-doped samples. The *S* values of all the samples are negative over the whole temperature range examined, indicating n-type conduction. As shown in the inset of Fig. 4, at 1173 K, the α/γ-Al_2O_3-doped samples exhibit a monotonic decrease of *S* with increasing calcination temperature. According to Jonker and the Pisarenko relation, a simple broad band model for extrinsic n-type semiconductors with negligible hole conduction can describe this behavior [12],

$$\sigma = ne\mu \qquad (2)$$

$$|S| = A'Tm_d^* \left(\frac{\pi}{3n}\right)^{2/3} \qquad (3)$$

where *n* is the carrier concentration, *e* is the electric charge of the carrier, μ is the mobility, *A'* is a constant, *T* is the absolute temperature, m_d^* is a density of the state (DOS) effective mass at the Fermi level. As the electrical conductivity (σ) and the Seebeck coefficient (*S*) are both a function of the carrier concentration (*n*), Eq. 2 and 3 clearly show that a higher *n* value causes an increase in σ but a decrease in |*S*|, which well explains the tendency observed in Fig.4. For example, the α-1273 sample with the highest electrical conductivity showed the smallest |*S*| in the investigated temperature region.

The total thermal conductivity (κ) of the sintered samples using different α/γ-Al_2O_3 and various calcination temperatures is shown in Fig. 5. In general, κ rapidly decreases with increasing temperature, which is in good agreement with the result reported by Ohtaki et al [13]. It can also be seen from Fig. 5 that κ tends to increase with increasing calcination temperature. We estimated the electronic contribution κ_e using the Wiedemann–Franz law and found that the increase in κ with increasing calcination temperature is attributed to the increase in κ_e, particularly in the high temperature region. Although the total κ values at 1173 K

as a function of the calcination temperature (see Fig. 5 inset) appeared to be virtually the same for both α- and γ-Al_2O_3-doped samples, the lattice thermal conductivity, κ_L, of the samples at 1173 K was somewhat smaller for the γ-1073 and γ-1173 samples (5.06 $Wm^{-1}K^{-1}$ and 5.15 $Wm^{-1}K^{-1}$, respectively) than those of the α-1073 α-1173 samples (5.31 $Wm^{-1}K^{-1}$ and 5.43 $Wm^{-1}K^{-1}$, respectively). As illustrated by the microstructure in Fig. 2, the reason for the lower conductivity in the γ-1073 sample as compared with the α-1073 sample is probably due to the formation of disperse $ZnAl_2O_4$ nanoprecipitates in γ-1073 sample which might act as a phonon scattering center.

The power factor, $S^2\sigma$, of the samples is presented in Fig. 6. It shows that the power factor values of γ-1073 and γ-1173 are notably higher than that of α-1073 and α-1173. Also, the power factor monotonically increases with increasing calcination temperature, as shown in the inset of Fig. 6. The higher power factor observed for the γ-Al_2O_3-doped samples was mainly due to the increase in their electrical conductivity as compared to that of the α-Al_2O_3-doped samples. At 1173K, the highest power factor of ~$8.31\times10^{-4}Wm^{-1}K^{-2}$ measured in this study is comparable to the value of ~$8 – 15\times10^{-4}$ $Wm^{-1}K^{-2}$ reported by Ohtaki et al [1] and the value of ~$8.3\times10^{-4}Wm^{-1}K^{-2}$ reported by Jood et al [2] for Al-doped ZnO.

The dimensionless figure of merit, *ZT*, is given in Fig. 7, showing that the *ZT* values of γ-1073 and γ-1173 are also higher than those of α-1073 and α-1173. At 1173K, the γ-1173 sample with the highest power factor attained a *ZT* of 0.17, which is about 27% higher than that for the α-Al_2O_3-doped counterpart at the same temperature. The highest ZT value of our sample is on the same order of the one reported by Ohtaki et al [1] at the same temperature. It should be noted here that the higher ZT value (ZT ~ 0.44 at 1000 K) reported by Jood et al is mainly due to the suppression in the thermal conductivity of the sample by nanostructuring [2]. Nevertheless, our ZT value is higher than the ones reported by Cai et al [10] and Tanaka et al [16] at the same temperature.

We found that the ZnO samples doped with γ-Al_2O_3 showed a better thermoelectric performance compared to those doped with α-Al_2O_3, when calcined at a temperature lower than 1273 K. At a calcination temperature higher than 1273 K, the difference in the thermoelectric properties gradually diminishes due to the intrinsic phase transformation of γ-Al_2O_3 to α-Al_2O_3.

To understand these observations, we looked into the kinetics and mechanism of the reaction between ZnO and Al_2O_3. The formation of the secondary phase, $ZnAl_2O_4$, resulting from the reaction between ZnO and Al_2O_3 is well known, and can be represented as follows:

$$ZnO + Al_2O_3 \rightarrow ZnAl_2O_4 \qquad (4)$$

It should be noted that the formation of $ZnAl_2O_4$ cannot be avoided during the preparation process of Al-doped ZnO [2,4,5]. The limited solubility of Al atom into ZnO [14] could be one of the reasons. According to the thermodynamics description of the reaction (Eq. 4) suggested by K. T. Jacob [6], the standard Gibbs free energy change (ΔG) of the $ZnAl_2O_4$ formation from the reaction of α-Al_2O_3 and ZnO equals -45.0081+0.0066T kJ, indicating that the formation of $ZnAl_2O_4$ is favored from room temperature to far above 1673 K (ΔG □ 0). The reaction rate is kinetically controlled by solid state diffusion [7,8].

Fig. 8 shows the calculated reaction time course of $ZnAl_2O_4$ formation using Jander's model for powder reactions. According to this model, it is assumed that Al_2O_3 particles are embedded in a quasi-continuous ZnO medium. The reaction rate of the $ZnAl_2O_4$ formation from ZnO and Al_2O_3 is diffusion-controlled and hence follows a parabolic rate law:

$$\left[1-(1-W)^{\frac{1}{3}}\right]^2 = 2 \cdot k_p \cdot t/r_o^2 \qquad (5)$$

where W is the weight fraction of the reacted Al_2O_3, k_p is the practical parabolic rate constant, t is the reaction time and r_o is the particle size of Al_2O_3 powder. The practical parabolic rate constant k_p follows the Arrhenius law:

$$k_p = A \cdot e^{-\frac{E_a}{RT}} \qquad (6)$$

where A is pre-exponential factor (a term which includes factors like the frequency of collisions and their orientation), E_a is the activation energy, R is the gas constant, T is temperature. By combining Eq. 5 and Eq. 6, one can obtain:

$$W = 1-[1-(2A \cdot t)^{\frac{1}{2}} \cdot e^{-\frac{E_a}{2RT}} \cdot r_o^{-1}]^3 \qquad (7)$$

According to the experimental data reported by Tsuchida et al [8], the parameters of A and E_a can be obtained by Arrhenius fitting. A equals 18076 μm^2 min^{-1}. E_a for α-Al_2O_3 and γ-Al_2O_3 equals 4.9 and 2.04 eV, respectively. r_o equals the average particle size of Al_2O_3 powder. Using Eq. 7, the reacted Al_2O_3 fraction can be

plotted as a function of time. As shown in Fig. 8a, the reaction rate of γ-Al_2O_3 with ZnO is significantly higher than that of α-Al_2O_3 at the same temperature due to the lower activation energy of γ-Al_2O_3. From these data, we calculated the percentage of reaction completed after1 hour as a function of the calcination temperature, and the results are shown in Fig. 8b. A clear correlation was found between the percentage of the reacted Al_2O_3 and the thermoelectric properties of these samples. The α-1073 sample with the smallest calculated percentage of the reacted Al_2O_3 showed the lowest σ values, while the α-1273 and γ-1173 samples with almost fully reacted Al_2O_3 showed relatively high σ. Accordingly, the electrical conductivities of the γ-1073/1173 samples were higher than those of the α-1073/1173 samples (Fig. 3). Also, the smaller grains size of the γ-Al_2O_3-doped samples compared to that of the α-Al_2O_3-doped ones may be explained by a stronger boundary pinning effect during grain growth caused by a larger number of $ZnAl_2O_4$ nanoprecipitates. This is presumably due to the faster reaction and larger fraction of $ZnAl_2O_4$ formation for the γ-Al_2O_3-doped samples.

The detailed mechanisms of the reaction between ZnO and Al_2O_3 have already been studied by Branson [7] and Tsuchida et al [8]. Branson carried out marker transport experiments at the interfaces between ZnO, $ZnAl_2O_4$ and Al_2O_3, and pointed out that the formation of $ZnAl_2O_4$ is a result of Zn ions diffusing into Al_2O_3. Later, Tsuchida et al. not only showed evidence to support this result but also revealed the reason for the $ZnAl_2O_4$ formation speed. They pointed out that the reaction of α or γ-Al_2O_3 with ZnO resulted in different degrees of crystallinity of the product layers, i.e. formation of $ZnAl_2O_4$ as “hereditary structure” [8]. Owing to the different degrees of crystallinity, the diffusivity of Zn ions in $ZnAl_2O_4$ can be varied. As a result, in the γ-Al_2O_3, the formation of a defect $ZnAl_2O_4$ layer with a higher diffusivity of the Zn ions is observed. Correspondingly, α-Al_2O_3 results in a nearly perfect, defect free $ZnAl_2O_4$ structure with a lower diffusivity of the Zn ions and higher activation energy.

However, the faster formation of the $ZnAl_2O_4$ phase is not likely to be the direct reason for the increase of the electrical conductivity in the γ-Al_2O_3-doped samples, since the $ZnAl_2O_4$ phase is reported to be unfavorable for the electrical conductivity [1]. By comparing Fig. 1b and 8b, the unit cell volume shrinkage increases along with increasing the $ZnAl_2O_4$ phase formation, indicating that the

substitution of Al for Zn simultaneously occurred during the formation of the $ZnAl_2O_4$ phase, which can be represented as:

$$Al_{Al}^{X} + \frac{1}{2}O_2 \xrightarrow{Z_n O} Al_{Z_n}^{\cdot} + O_o^X + e' \quad (8)$$

According to the previous investigations by Branson, the diffusion of Al toward ZnO does not contribute to the formation of $ZnAl_2O_4$ [7]. His explanation of the reaction between ZnO and Al_2O_3 did not take the Al diffusion into consideration. From our experimental results and investigations by other groups who observed the existence of Al diffusion into ZnO using HRTEM [15], a modified Branson's schematic diagram of the reaction process is proposed and the details is presented in Fig. 9. It includes a counter-diffusion between ZnO and Al_2O_3. The formation of $ZnAl_2O_4$ is only caused by the diffusion of Zn to Al_2O_3, while the Al substitution for Zn results from the diffusion of Al into ZnO. The disordered structure of γ-Al_2O_3 may lead to the disordered product layers of $ZnAl_2O_4$. The Al and Zn ions would be easier to diffuse through the disordered product layer. It promotes both the formation of $ZnAl_2O_4$ and the substitutions of Al for Zn as donor impurities in ZnO, thus resulting in enhanced grain boundary pinning by $ZnAl_2O_4$ and the observed higher electrical conductivity of the γ-Al_2O_3-doped ZnO than that of the α-Al_2O_3-doped counterpart.

4. Conclusions

In summary, we observed a close correlation between the thermoelectric properties, microstructure evolution, and the solid state reaction kinetics of the $ZnAl_2O_4$ formation using Jander's solid-state reaction model. At a given calcinations temperature, the addition of γ-Al_2O_3 resulted in a larger fraction of the $ZnAl_2O_4$ formation in the Al-doped ZnO samples, which also inhibited the grain growth and slightly reduced the lattice thermal conductivity. The higher diffusion rate of Al observed for the γ-Al_2O_3 resulted in a larger unit cell volume shrinkage and higher electrical conductivity as compared with the α-Al_2O_3-doped ZnO. As a consequence, γ-Al_2O_3-doped ZnO exhibited a higher ZT than the α-Al_2O_3-doped counterpart under the same preparation conditions with calcination temperatures lower than 1273 K.

Acknowledgements

The authors would like to thank the Programme Commission on Energy and Environment (EnMi) which is part of the Danish Council for Strategic Research (Contract No. 10-093971) for sponsoring the OTE-POWER research work.

References

[1] M. Ohtaki, T. Tsubota, K. Eguchi, H. Arai, High-temperature thermoelectric properties of $(Zn_{1-x}Al_x)O$, J. Appl. Phys. 79 (1997) 1816-1818.

[2] P. Jood, R. J. Mehta, Y. Zhang, G. Peleckis, X. Wang, R. W. Siegel, T. Borca-Tasciuc, S. X. Dou, G. Ramanath, Al-doped zinc oxide nanocomposites with enhanced thermoelectric properties, Nano Lett. 11 (2011) 4337–4342.

[3] K. H. Kim, S. H. Shim, K. B. Shim, Microstructural and thermoelectric characteristics of zinc oxide-based thermoelectric materials fabricated using a spark plasma sintering process, J. Am. Ceram. Soc. 88 (2005) 628–632.

[4] N. Ma, J. F. Li, B. P. Zhang, Y. H. Lin, L. R. Ren, G. F. Chen, Microstructure and thermoelectric properties of $Zn_{1-x}Al_xO$ ceramics fabricated by spark plasma sintering, J. Phys. and Chem. of Solids 71 (2012) 1344–1349.

[5] D. Berardan, C. Byl, N. Dragoe, Influence of the preparation conditions on the thermoelectric properties of Al-doped ZnO, J. Am. Ceram. Soc. 93 (2010) 2352–2358.

[6] K. T. Jacob, Gibbs free energies of formation of $ZnAl_2O_4$ and $ZnCr_2O_4$, Thermochimica Acta 15 (1976) 79-87.

[7] D. L. Branson, Kinetics and mechanism of the reaction between zinc oxide and aluminum oxide, J. Am. Ceram. Soc. 48 (1965) 591.

[8] T. Tsuchida, R. Furuichi, T. Ishii, Reactivity of η-, γ-, and α-Al_2O_3 for $ZnAl_2O_4$ formation, Z anorg. Allg. Chem. 415 (1975) 175-184.

[9] N. Moelans, B. Blanpain, P. Wollants, Pinning effect of second-phase particles on grain growth in polycrystalline films studied by 3-D phase field simulations, Acta Mater. 55 (2007) 2173-2182.

[10] K. F. Cai, E. Muller, C. Drasar, A. Mrotzek Preparation and thermoelectric properties of Al-doped ZnO ceramics, Mater. Sci. Eng. B 104 (2003) 45–48.

[11] A. E. Jimenez-Gonzalez, J. A. S. Urueta, R. Suarez-Parra, Optical and electrical characteristics of aluminum-doped ZnO thin films prepared by solgel technique, J. Cryst, Growth 192 (1998) 430–438.

[12] M. Y. Su, C. E. Elsbernd, T. O. Mason, Jonker 'Pear' Analysis of Oxide Superconductors, J. Am. Ceram. Soc. 73 (1990) 415-419.

[13] M. Ohtaki, K. Araki, K. Yamamoto, High thermoelectric performance of dually doped ZnO ceramics, J. Electron Mater. 38 (2009) 1234.

[14] H. Serier, M. Gaudon, M. Ménétrier, Al-doped ZnO powdered materials: Al solubility limit and IR absorption properties, Solid State Sci. 11 (2009) 1192-1197.

[15] Y. Kinemuchi, H. Nakano, H. Kaga, S. Tanaka, K. Uematsu, K. Watari, Microstructural evidence of hall mobility anisotropy in c-axis textured Al-doped ZnO, J. Am. Ceram. Soc. 94 (2011) 2339-2343.

[16] Y. Tanaka, T. Ifuku, K. Tsuchida, A. Kato, Thermoelectric properties of ZnO-based materials, J. Mater. Sci. Lett. 16 (1997) 155.

[17] R. D. Shannon, Revised Effective Ionic Radii and Systematic studies of interatomic distances in halides and chalcogenides, Acta Cryst. A 32 (1976) 751.

[18] N. Vogel-Schäuble, Y. E. Romanyuk, S. Yoon, K. J. Saji, S. Populoh, S. Pokrant, M. H. Aguirre, A. Weidenkaff, Thermoelectric properties of nanostructured Al-substituted ZnO thin films, thin solid film 520 (2012) 6869-6875.

Figure captions

Fig. 1. (a) XRD patterns of α/γ-Al_2O_3-doped ZnO with different calcination temperatures (from 973 to 1273 K). The dotted box magnified as the inset shows the position of the strongest peak from $ZnAl_2O_4$. (b) The unit cell volume obtained from the lattice parameter refinement as a function of the calcination temperature.

Fig. 2. SEM photographs of the fracture surfaces of α/γ-Al_2O_3-doped ZnO. (a) γ-973, (b) γ-1073, (c) α-1073, (d) α-1273, (e) a representative high-magnification SEM image of the $ZnAl_2O_4$ nanoprecipitates. EDX line scans of Zn, O, and Al $K\alpha_1$ X-ray peaks obtained along the yellow arrow are shown in (f).

Fig. 3. Temperature dependence of the electrical conductivity of α/γ-Al_2O_3-doped ZnO samples. The inset shows the electrical conductivity at 1173 K as a function of the calcination temperature.

Fig. 4. Temperature dependence of the Seebeck coefficient of α/γ-Al_2O_3-doped ZnO samples. The inset shows the Seebeck coefficient at 1173 K as a function of the calcination temperature.

Fig. 5. Temperature dependence of the thermal conductivity of α/γ-Al_2O_3-doped ZnO samples. The inset shows the thermal conductivity at 1173 K as a function of the calcination temperature.

Fig. 6. Temperature dependence of the power factor of α/γ-Al_2O_3-doped ZnO samples. The inset shows the power factor at 1173 K as a function of the calcination temperature.

Fig. 7. Temperature dependence of ZT of α/γ-Al_2O_3-doped ZnO samples. The inset shows the ZT values at 1173 K as a function of the calcination temperature.

Fig.8. (a) The calculated reaction time course as a weight fraction of reacted Al_2O_3 for the $ZnAl_2O_4$ formation. (b) The percentage of reaction completed after1 hour as a function of the calcination temperature.

Fig. 9. A modified schematic diagram for the solid-state reaction process of ZnO and Al_2O_3 based on Branson's investigation.

359

360 Fig. 1

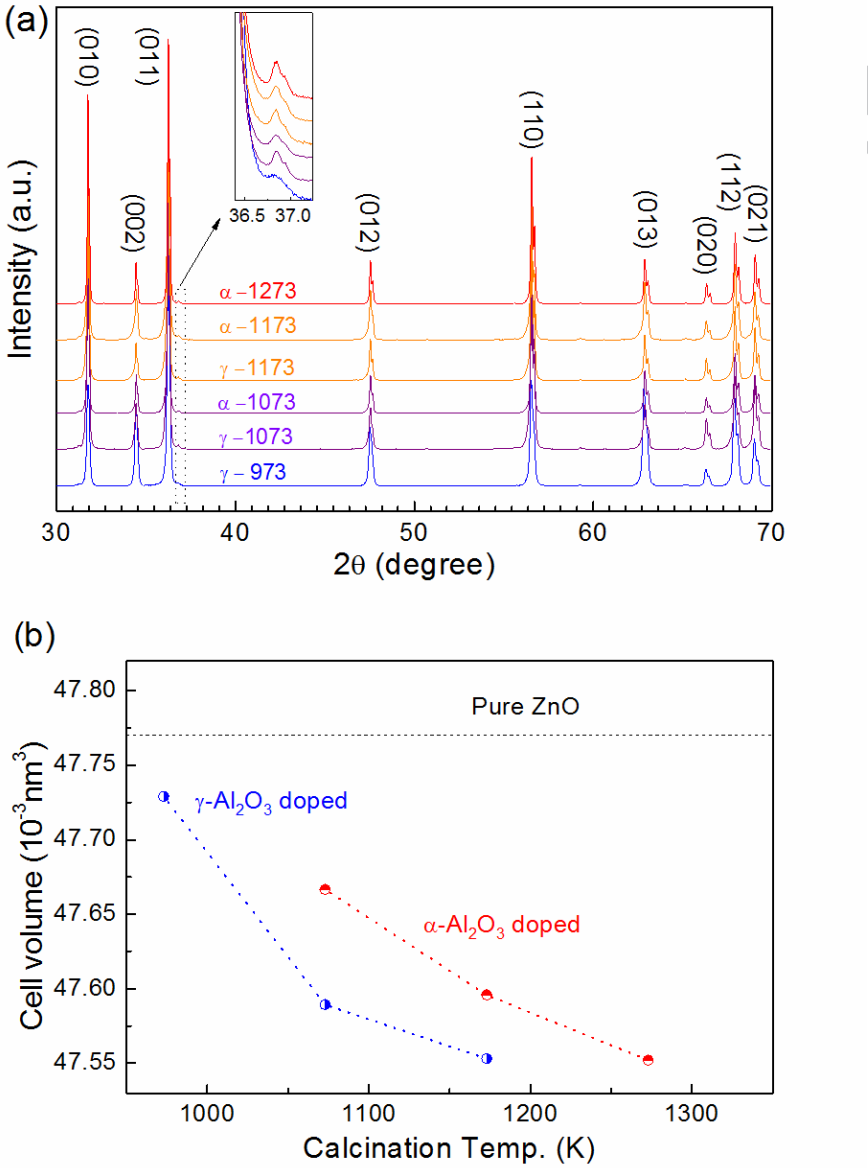

361

362 Fig. 1. (a) XRD patterns of α/γ-Al_2O_3-doped ZnO with different calcination temperatures (from
363 973 to 1273 K). The dotted box magnified as the inset shows the position of the strongest peak
364 from $ZnAl_2O_4$. (b) The unit cell volume obtained from the lattice parameter refinement as a
365 function of the calcination temperature.

366

367 Fig. 2

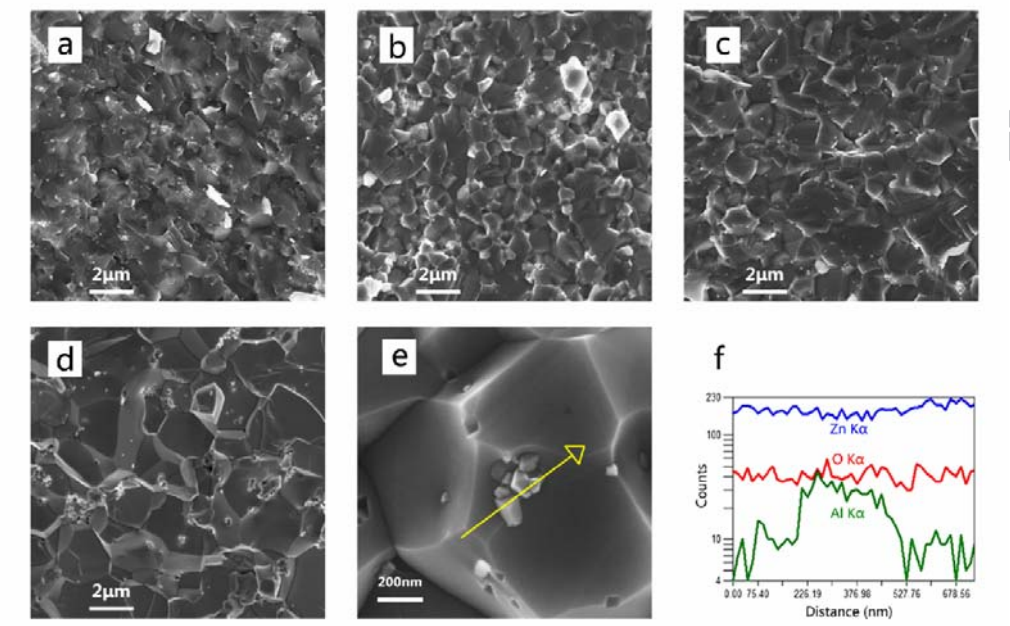

368

369 Fig. 2. SEM photographs of the fracture surfaces of α/γ-Al_2O_3-doped ZnO. (a) γ-973, (b) γ-1073,
370 (c) α-1073, (d) α-1273, (e) a representative high-magnification SEM image of the $ZnAl_2O_4$
371 nanoprecipitates. EDX line scans of Zn, O, and Al $K\alpha_1$ X-ray peaks obtained along the yellow
372 arrow are shown in (f).

373

374 Fig. 3

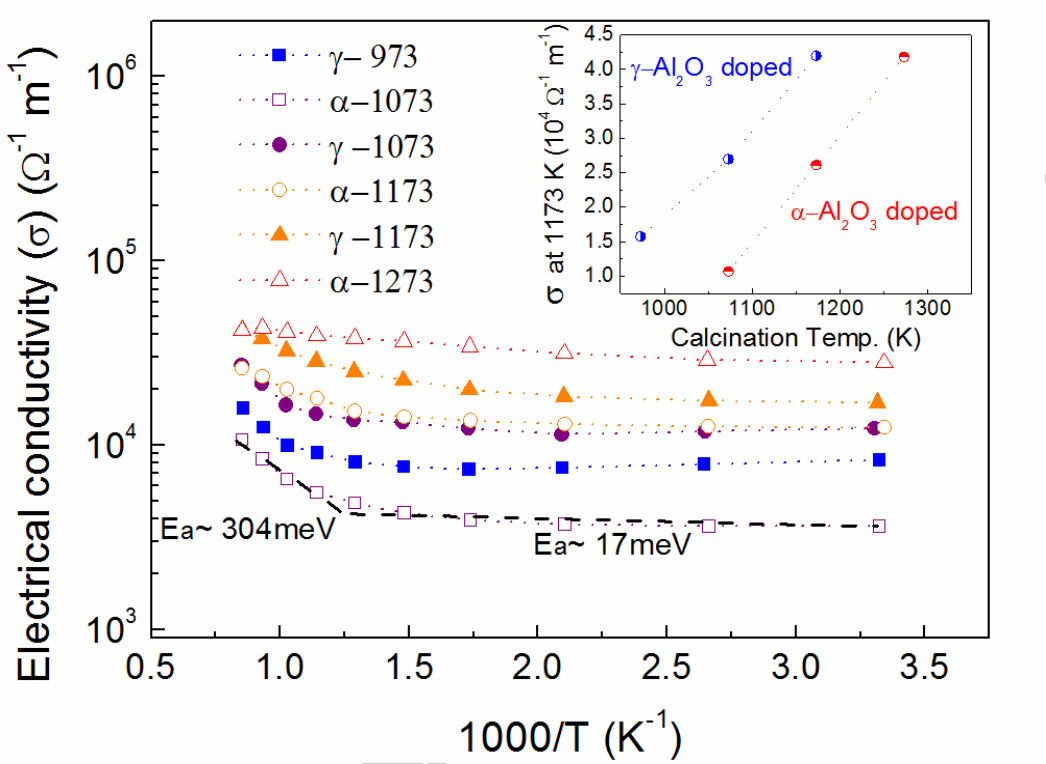

375

376 Fig. 3. Temperature dependence of the electrical conductivity of α/γ-Al_2O_3-doped ZnO samples.
377 The inset shows the electrical conductivity at 1173 K as a function of the calcination temperature.
378

379 Fig. 4

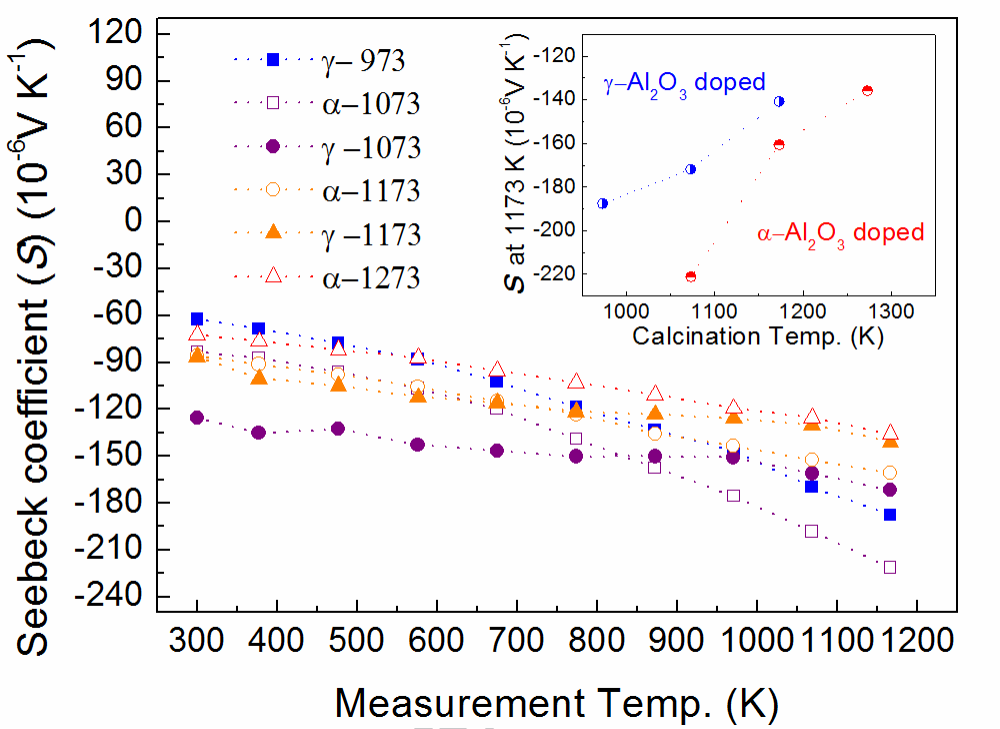

380

381 Fig. 4. Temperature dependence of the Seebeck coefficient of α/γ-Al_2O_3-doped ZnO samples. The
382 inset shows the Seebeck coefficient at 1173 K as a function of the calcination temperature.
383

384 Fig. 5

385

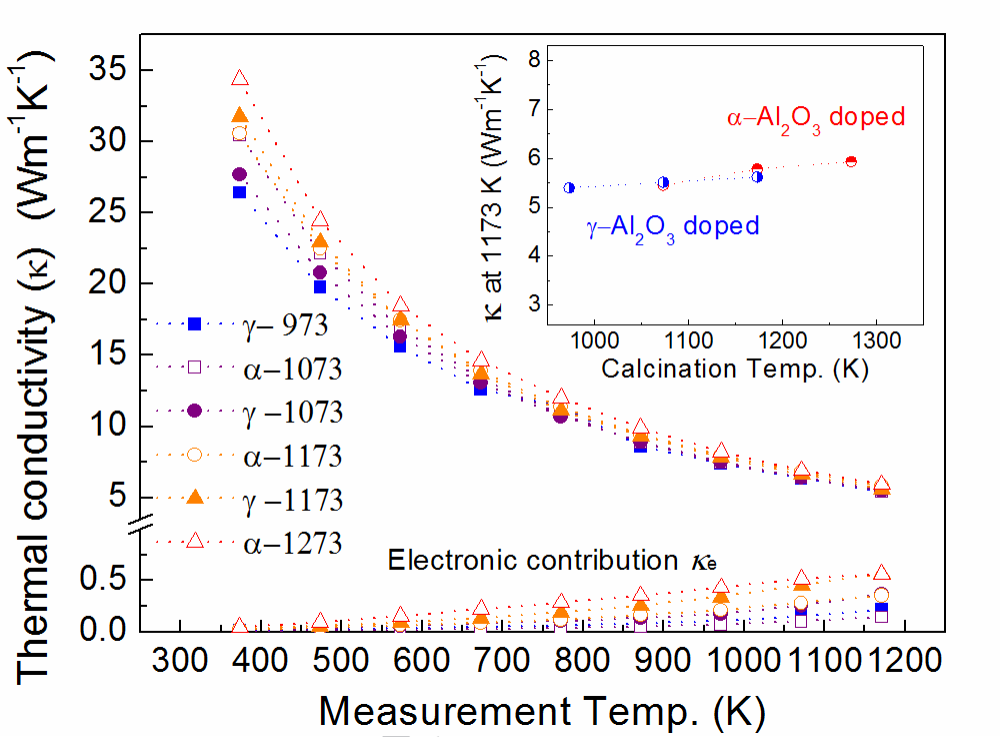

386

387 Fig. 5. Temperature dependence of the thermal conductivity of α/γ-Al_2O_3-doped ZnO samples.

388 The inset shows the thermal conductivity at 1173 K as a function of the calcination temperature.

389

390 Fig. 6

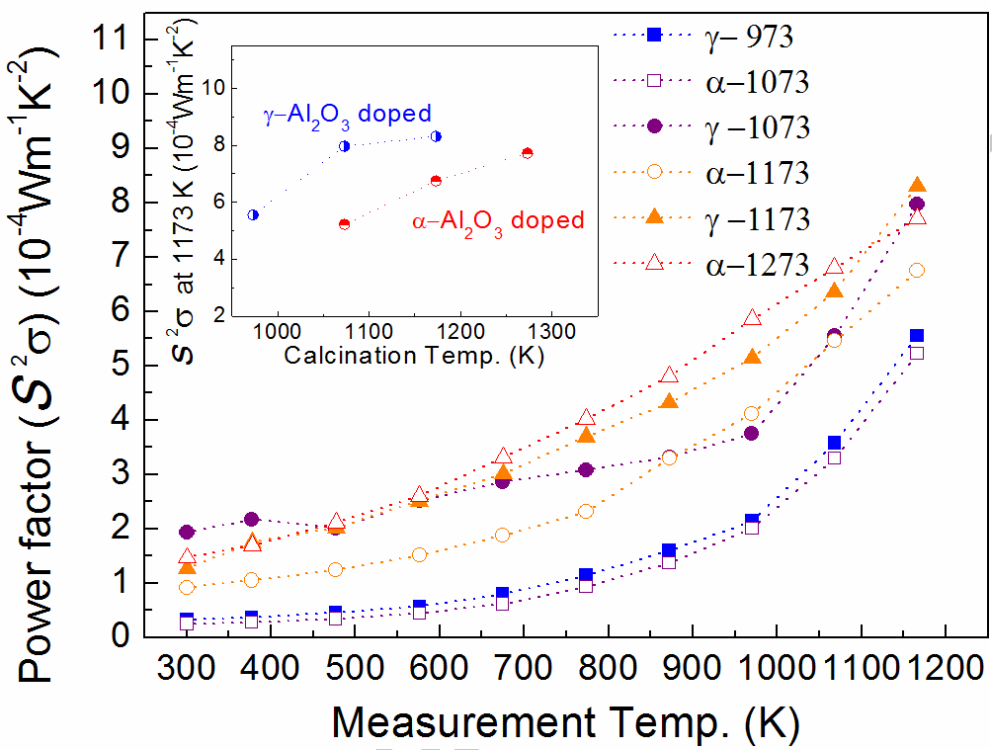

391

392 Fig. 6. Temperature dependence of the power factor of α/γ-Al_2O_3-doped ZnO samples. The inset
393 shows the power factor at 1173 K as a function of the calcination temperature.

394

395 Fig. 7

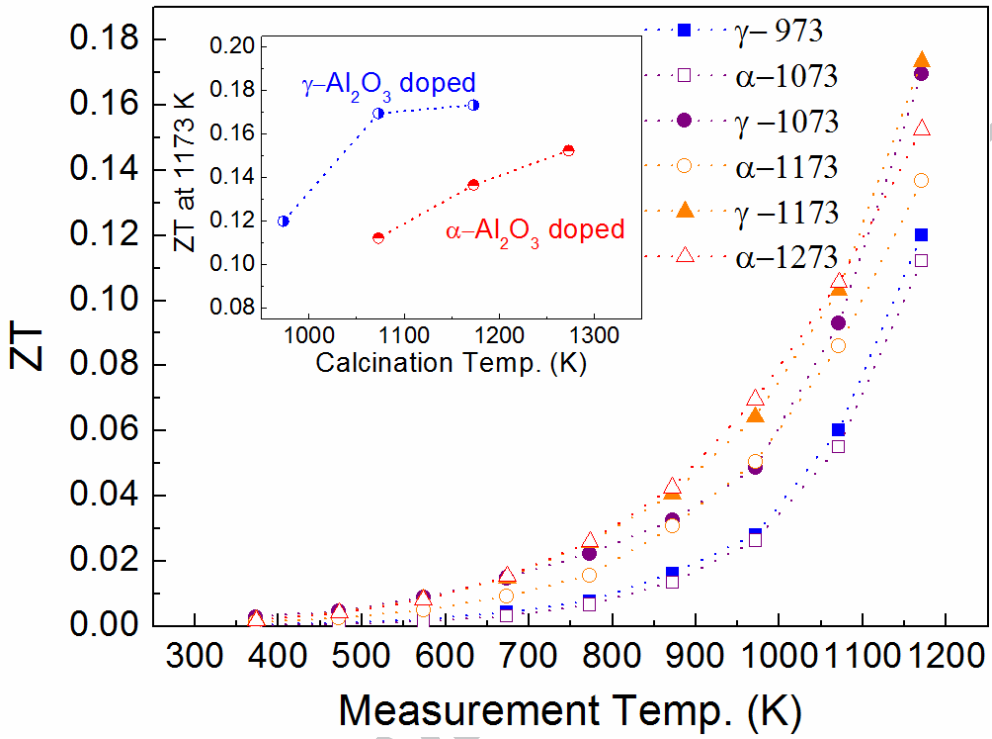

396

397 Fig. 7. Temperature dependence of ZT of α/γ-Al_2O_3-doped ZnO samples. The inset shows the ZT
398 values at 1173 K as a function of the calcination temperature.

399

400 Fig. 8

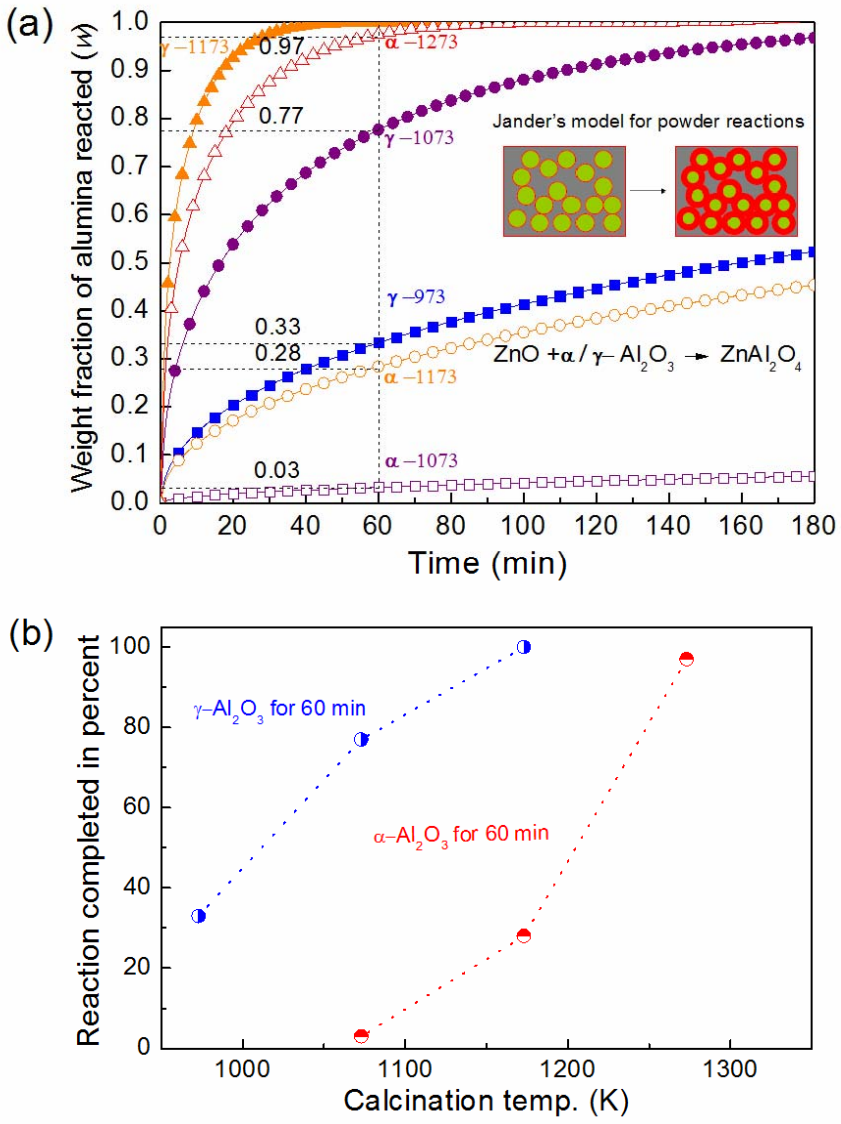

401

402 Fig.8. (a) The calculated reaction time course as a weight fraction of reacted Al_2O_3 for the
403 $ZnAl_2O_4$ formation. (b) The percentage of reaction completed after1 hour as a function of the
404 calcination temperature.

405

406

407 Fig. 9

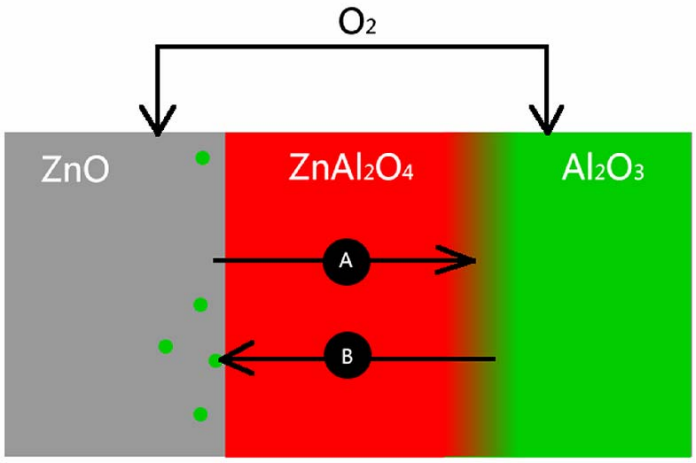

$$A: \quad Zn^{2+} + 2e' + \frac{1}{2}O_2 + Al_2O_3 \rightarrow ZnAl_2O_4$$

$$B: \quad Al_{Al}^{X} + \frac{1}{2}O_2 \xrightarrow{Zn O} Al_{Zn}^{\cdot} + O_o^X + e'$$

408

409 Fig. 9. A modified schematic diagram for the solid-state reaction process of ZnO and Al_2O_3 based
410 on Branson's investigation.

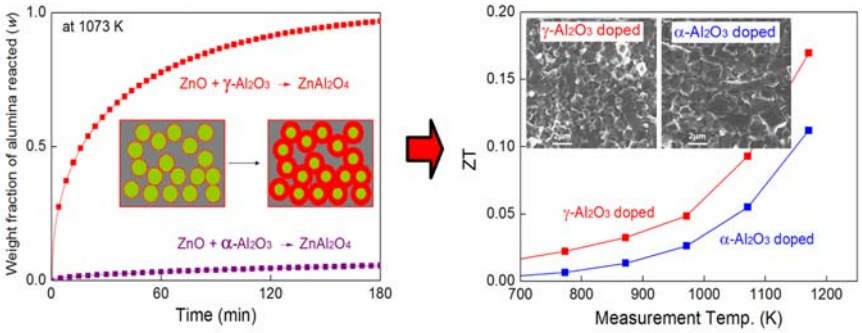

411

Highlights

- Clear differences in microstructure and thermoelectric properties were observed between the γ-Al_2O_3-doped ZnO and α-Al_2O_3-doped ZnO.
- γ-Al_2O_3-doped ZnO obtained a higher ZT than that of α-Al_2O_3-doped ZnO with the same preparation condition lower than 1273K.
- The differences in microstructure and thermoelectric properties with α-/ γ-Al_2O_3-doped ZnO can be correlated to the solid state reaction kinetics of $ZnAl_2O_4$ formation.
- A possible mechanism of $ZnAl_2O_4$ formation was proposed.